Mini-soliton stars

R. Friedberg, T. D. Lee, and Y. Pang
Columbia University, New York, New York 10027
(Received 28 October 1986)

Nontopological soliton solutions of a complex scalar field in general relativity are derived. The theory is renormalizable (except for graviton loops), and these solutions are valid both classically and quantum mechanically. We study the ground states (which are stable) as well as the excited states, but restrict ourselves to spherically symmetric ones. Their physical characteristics can be rather remarkable. For example, if the mass of the scalar field is about 30 GeV, then a mini-soliton star could have a radius $\sim 6\times 10^{-16}$ cm, a mass $\sim 10^{10}$ kg, and a density $\sim 10^{41}$ times that of a neutron star.

I. INTRODUCTION

In the preceding paper,[1] it was pointed out that the extension of the nontopological soliton to include gravity can lead to new possibilities for cold stable stellar configurations, called soliton stars. The simplest of these is the mini-soliton star, whose structure will be analyzed in this paper. Consider the case of a complex spin-0 field ϕ of mass $m\neq 0$ in general relativity, with no direct meson-meson coupling, or only repulsive coupling (as would be the case if there is no other field and the theory is renormalizable). The theory is assumed to be invariant under a space-independent phase transformation

$$\phi\rightarrow e^{i\theta}\phi\ ; \tag{1.1}$$

consequently, we have the conservation of its generator N, called the particle number. Mini-soliton stars refer to those stable configurations with very large N. As we shall examine in detail, such an object has a miniscule spatial dimension $\sim m^{-1}$, like an elementary particle; but its mass M can be rather large, typically about (in units $\hbar=c=1$)

$$\sim (l_P m)^{-2} m\ , \tag{1.2}$$

where $l_P\sim 10^{-33}$ cm is the Planck length. Take the example of $m\sim 30$ GeV: (1.2) means that the extension of the mini-soliton star is $\sim 6\times 10^{-16}$ cm, but its mass can be $\sim 10^{10}$ kg, with an $N\sim 10^{35}$ and a density $\sim 10^{41}$ times that of a neutron star.

For the ground state, there is the inequality

$$M<Nm\ , \tag{1.3}$$

which ensures its stability against decaying into N free particles.

In the following, we shall restrict our investigation to spherically symmetric solutions; the square of length differential can be written in terms of the spherical coordinates (t,ρ,α,β) as

$$ds^2=-e^{2u}dt^2+e^{2\bar{v}}d\rho^2+\rho^2(d\alpha^2+\sin^2\alpha\, d\beta^2) \tag{1.4}$$

or in terms of the isotropic coordinates (t,r,α,β) as

$$ds^2=-e^{2u}dt^2+e^{2v}(dr^2+r^2d\alpha^2+r^2\sin^2\alpha\, d\beta^2)\ , \tag{1.5}$$

where α,β are the standard polar and azimuthal angles, and ρ is $(2\pi)^{-1}$ times the circumference (i.e., the length of the great circle) of a two-sphere, related to r by

$$\rho=re^{v}\ . \tag{1.6}$$

The functions u, v, and $\bar{v}$ depend only on r, or, equivalently, only on ρ. Hence,

$$e^{-\bar{v}}=d\ln\rho/d\ln r=1+r\frac{dv}{dr}\ . \tag{1.7}$$

The invariant volume element is

$$d\tau=|g|^{1/2}\prod_{\mu=0}^{3}dx^{\mu}$$
$$=|g|^{1/2}dt\,dx^1dx^2dx^3\ , \tag{1.8}$$

where $dx^0=dt$ and $|g|$ is the absolute value of the metric determinant. For the two coordinates (1.4) and (1.5), we have

$$|g|^{1/2}dx^1dx^2dx^3=e^{u+\bar{v}}\rho^2\sin\alpha\, d\rho\, d\alpha\, d\beta \tag{1.9}$$

in the former, and

$$|g|^{1/2}dx^1dx^2dx^3=e^{u+3v}r^2\sin\alpha\, dr\, d\alpha\, d\beta \tag{1.10}$$

in the latter. Both coordinate systems are useful. Quite often they will be used concurrently.

Consider a large two-sphere of a constant circumference $2\pi\rho_0$ (which will $\rightarrow\infty$ in the end). Let $A(g)$ be the gravitational action over a four-dimensional region Ω, whose boundary S is the product of the time axis with the two-sphere:

$$\rho=\rho_0\ . \tag{1.11}$$

We may write, in addition to Hilbert's action, a surface term[2]

$$A(g)=(16\pi G)^{-1}\left[\int_{\Omega}\mathscr{R}\,d\tau+\int_{S}\mathscr{S}\,dS\right]\ , \tag{1.12}$$

where $\mathscr{R}$ is the scalar curvature,

$$\mathscr{S} \equiv 2n^{\mu}{}_{;\mu} - (4/\rho_0) \tag{1.13}$$

with $n^{\mu}{}_{;\mu}$ the covariant divergence of the (four-dimensional) unit vector n^{μ}, normal to the surface S, and dS is the invariant surface element on S, so that (at points on the surface)

$$n^{\mu} n_{\mu} = 1 \tag{1.14}$$

and

$$n_{\mu} dx^{\mu} dS = d\tau \ . \tag{1.15}$$

For example, in the spherical coordinates (t,ρ,α,β) the only nonzero component of n_{μ} is

$$n_{\rho} = e^{\bar{v}} ; \tag{1.16}$$

this gives $n^{\rho} = e^{-\bar{v}}$ and [by extending the definition (1.16) of n_{μ} also to points adjacent to S]

$$n^{\mu}{}_{;\mu} = e^{-\bar{v}} \left[\frac{du}{d\rho} + \frac{2}{\rho} \right] . \tag{1.17}$$

Hence, on the surface S, we have

$$\mathscr{S} = 2e^{-\bar{v}} \frac{du}{d\rho} + \frac{4}{\rho}(e^{-\bar{v}} - 1) \ , \tag{1.18}$$

where $\rho = \rho_0$. Because of (1.15),

$$e^{\bar{v}} d\rho \, dS = e^{u+\bar{v}} \rho^2 \sin\alpha \, dt \, d\rho \, d\alpha \, d\beta \ , \tag{1.19}$$

which gives

$$dS = e^{u} \rho^2 \sin\alpha \, dt \, d\alpha \, d\beta \ . \tag{1.20}$$

Likewise, in the isotropic coordinates (t,r,α,β) the only nonzero component of n_{μ} is $n_r = e^{v}$, which gives $n^{r} = e^{-v}$ and

$$n^{\mu}{}_{;\mu} = e^{-v} \left[\frac{du}{dr} + 2\frac{dv}{dr} + \frac{2}{r} \right] . \tag{1.17'}$$

Therefore, (1.18)—(1.20) become

$$\mathscr{S} = 2e^{-v} \left[\frac{du}{dr} + 2\frac{dv}{dr} \right] , \tag{1.18'}$$

$$e^{v} dr \, dS = e^{u+3v} r^2 \sin\alpha \, dt \, dr \, d\alpha \, d\beta \ , \tag{1.19'}$$

and

$$dS = e^{u+2v} r^2 \sin\alpha \, dt \, d\alpha \, d\beta \ . \tag{1.20'}$$

Clearly, expressions (1.17)—(1.20) are identical to (1.17')—(1.20'). For the time-independent metric $g_{\mu\nu}$ that we are considering, the t integration is a trivial one. We may write

$$A(g) = L(g) \int dt \ , \tag{1.21}$$

where $L(g)$ is the Lagrangian of the gravitational field. The corresponding gravitational energy is

$$E(g) = -L(g) \ .$$

By using (1.12)—(1.20), we find, in the spherical coordinates,

$$\begin{aligned} L(g) &= -E(g) \\ &= (2G)^{-1} \int e^{u} \left[e^{\bar{v}} - 2 \left[1 + \rho \frac{du}{d\rho} \right] \right. \\ &\quad \left. + e^{-\bar{v}} \left[1 + 2\rho \frac{du}{d\rho} \right] \right] d\rho \ . \end{aligned} \tag{1.22}$$

Similarly, in the isotropic coordinates,

$$L(g) = -E(g) = (2G)^{-1} \int e^{u+v}(2u'v' + v'^2) r^2 dr \ , \tag{1.22'}$$

where

$$u' = du/dr \quad \text{and} \quad v' = dv/dr \ . \tag{1.23}$$

The inclusion of the surface integration in (1.12) converts Hilbert's action into one that contains only the first derivative of the metric, so that the usual Lagrangian mechanics formulation can be applicable. For the two-sphere (1.11), its circumference $2\pi\rho_0$ is clearly an invariant quantity; therefore, $\mathscr{S}$, defined by (1.13), is manifestly invariant under any coordinate transformation in the four-dimensional space, like the scalar curvature $\mathscr{R}$.

For a complex field ϕ, the matter action is

$$A(m) = -\int [\phi^{\dagger\mu} \phi_{\mu} + U(\phi^{\dagger}\phi)] d\tau \ , \tag{1.24}$$

where $\phi^{\dagger}$ is the Hermitian conjugate of ϕ,

$$\begin{aligned} &\phi_{\mu} = \frac{\partial \phi}{\partial x^{\mu}} , \quad \phi^{\dagger}_{\mu} = \frac{\partial \phi^{\dagger}}{\partial x^{\mu}} \ , \\ &\phi^{\mu} = g^{\mu\nu} \phi_{\nu} , \quad \text{and} \quad \phi^{\dagger\mu} = g^{\mu\nu} \phi^{\dagger}_{\nu} \ . \end{aligned} \tag{1.25}$$

The current j^{μ}, defined by

$$j^{\mu} \equiv -i(\phi^{\dagger}\phi^{\mu} - \phi^{\dagger\mu}\phi) \ , \tag{1.26}$$

is conserved:

$$j^{\mu}{}_{;\mu} = 0 \ , \tag{1.27}$$

and therefore

$$\frac{\partial}{\partial x^{\mu}} (|g|^{1/2} j^{\mu}) = 0 \ . \tag{1.28}$$

A classical soliton solution is, by definition, *regular* everywhere, and it is zero at infinity ($r \to \infty$). Its amplitude is proportional to the inverse of some appropriate attractive-force coupling constant; in the case of the mini-soliton star, since the attraction is provided by the gravity, it is proportional to $G^{-1/2}$, as we shall see. In the weak-coupling limit $G \to 0$, the soliton amplitude ϕ diverges, which is typical. Once this singularity in coupling constant is factored out, a power-series expansion in the coupling constant can be established. The quantization and the formal quantum perturbative method can then be carried out for any soliton state in a straightforward way. Here, there is also no difficulty, except that the graviton-loop diagrams remain divergent (due to quantum fluctuations at distances $\sim$ the Planck length $l_P \ll m^{-1}$). Throughout the paper, we are concerned only with distances $\sim m^{-1}$ or larger. Ignoring graviton loops, a renormalizable quantum theory for the mini-soliton star can be obtained by following the well-established procedures[3] for quantum solitons, provided

$$U=m^2\phi^\dagger\phi+f^2(\phi^\dagger\phi)^2 . \tag{1.29}$$

Because the meson-meson coupling is repulsive in this case, the existence of soliton solutions depends only on Newton's constant G; the presence of f^2 is not an important feature. In what follows, we shall concentrate only on the classical solution, and refer the quantization to the standard literature.

As will be shown in the Appendix, at any given N, the minimum energy solution requires ϕ to have a harmonic dependence on t:

$$\phi\propto e^{-i\omega t} . \tag{1.30}$$

Hence the matter action becomes

$$A(m)=L(m)\int dt , \tag{1.31}$$

where

$$L(m)=\int(-U-V+W)\,|g|^{1/2}dx^1dx^2dx^3 . \tag{1.32}$$

For a spherically symmetric solution, we may write

$$\phi=2^{-1/2}\sigma e^{-i\omega t} , \tag{1.33}$$

where σ depends only on ρ (i.e., only on r). In terms of σ, the functions U, V, and W become

$$U=\tfrac{1}{2}m^2\sigma^2+\tfrac{1}{4}f^2\sigma^4 , \tag{1.34}$$

$$V=\tfrac{1}{2}e^{-2\bar v}\left[\frac{d\sigma}{d\rho}\right]^2=\tfrac{1}{2}e^{-2v}\left[\frac{d\sigma}{dr}\right]^2 , \tag{1.35}$$

and

$$W=\tfrac{1}{2}\omega^2e^{-2u}\sigma^2 . \tag{1.36}$$

The particle number N is

$$\begin{aligned}N&=\int j^0\,|g|^{1/2}dx^1dx^2dx^3\\&=(2/\omega)\int W\,|g|^{1/2}dx^1dx^2dx^3 .\end{aligned} \tag{1.37}$$

Define the matter energy $E(m)$ to be

$$\begin{aligned}E(m)&=N\omega-L(m)\\&=\int(U+V+W)\,|g|^{1/2}dx^1dx^2dx^3 .\end{aligned} \tag{1.38}$$

The total energy of the system is given by

$$E=E(g)+E(m)=N\omega-L , \tag{1.39}$$

where the total Lagrangian is

$$L=L(g)+L(m) . \tag{1.40}$$

The basic equations can be derived either by minimizing E with N fixed, or by taking the extremity of L with ω fixed. For a mini-soliton star, the solution is regular everywhere, with

$$\omega<m . \tag{1.41}$$

Therefore, at ∞,

$$\sigma=O(e^{-(m^2-\omega^2)^{1/2}r})\to 0 . \tag{1.42}$$

Likewise, u, v, and $\bar v$ approach the Schwarzschild solution (also exponentially): as $\rho\to\infty$,

$$\begin{aligned}e^u&\to\left[1-\frac{4a}{\rho}\right]^{1/2},\\e^{\bar v}&\to\left[1-\frac{4a}{\rho}\right]^{-1/2},\end{aligned} \tag{1.43}$$

i.e., as $r\to\infty$

$$\begin{aligned}e^u&\to\frac{r-a}{r+a},\\e^v&\to\left[\frac{r+a}{r}\right]^2,\end{aligned} \tag{1.44}$$

where

$$a=\tfrac{1}{2}GM . \tag{1.45}$$

These equations and other identities are discussed in Sec. II. Their Newtonian limits are given in Sec. III. The exact relativistic solutions (for $f=0$, but $m\neq 0$) are examined in Sec. IV. Even for such a "free" field theory with gravity, although the basic system is simple, the behavior of the stellar mass M versus the particle number N is surprisingly complex, as can be seen from the examples given in Figs. 1 and 2, where n denotes the number of nodes in σ. At a fixed N, the mini-soliton star is described by discrete levels (as typical for nontopological soliton solutions).

II. GENERAL DISCUSSIONS

A. Basic equations

Let $\mathscr{R}_{\mu\nu}$ be the Ricci tensor and $\mathscr{R}=g^{\mu\nu}\mathscr{R}_{\mu\nu}$ the scalar curvature. The Einstein equation relates

$$G_{\mu\nu}=\mathscr{R}_{\mu\nu}-\tfrac{1}{2}g_{\mu\nu}\mathscr{R}$$

to the matter tensor: in the spherical coordinates (t,ρ,α,β) we have

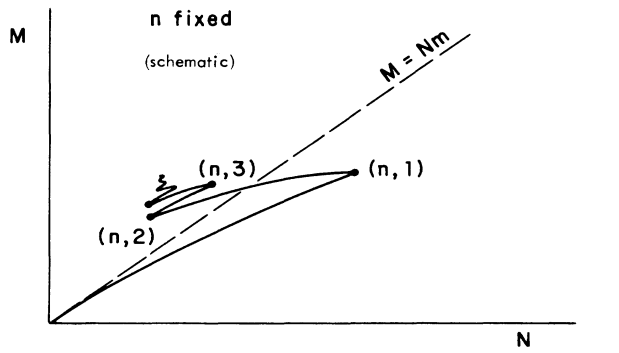

FIG. 1. A schematic drawing of the mass M of a spherically symmetric mini-soliton star vs its particle number N for a fixed number n of nodes (in the scalar field amplitude).

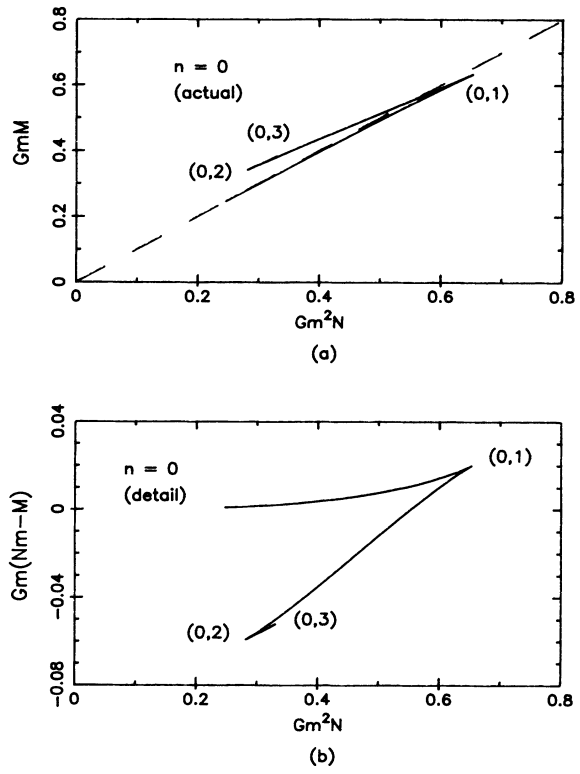

FIG. 2. Actual plot of the mass M vs the particle number N (a), and the binding energy $Nm-M$ vs N (b) for $n=0$.

$$\rho^2 G_t{}^t = e^{-2\bar{v}} - 1 - 2e^{-2\bar{v}}\rho\frac{d\bar{v}}{d\rho}$$
$$= -8\pi G\rho^2(W+V+U)\ , \tag{2.1}$$
$$\rho^2 G_\rho{}^\rho = e^{-2\bar{v}} - 1 + 2e^{-2\bar{v}}\rho\frac{du}{d\rho}$$
$$= 8\pi G\rho^2(W+V-U)\ , \tag{2.2}$$

and

$$\rho^2 G_\alpha{}^\alpha = e^{-2\bar{v}}\left[\rho^2\frac{d^2u}{d\rho^2} + \left[1+\rho\frac{du}{d\rho}\right]\rho\frac{d}{d\rho}(u-\bar{v})\right]$$
$$= 8\pi G\rho^2(W-V-U)\ ; \tag{2.3}$$

the last one is identical to that for $\rho^2 G_\beta{}^\beta$. The field equation of the spin-0 field,

$$e^{-2\bar{v}}\left[\frac{d^2\sigma}{d\rho^2} + \left[\frac{2}{\rho}+\frac{du}{d\rho}-\frac{d\bar{v}}{d\rho}\right]\frac{d\sigma}{d\rho}\right]$$
$$+\omega^2 e^{-2u}\sigma - \frac{dU}{d\sigma} = 0\ , \tag{2.4}$$

is related to Einstein's equations, on account of the identity

$$\frac{du}{d\rho}G_t{}^t - \left[\frac{2}{\rho}+\frac{du}{d\rho}+\frac{d}{d\rho}\right]G_\rho{}^\rho + \frac{2}{\rho}G_\alpha{}^\alpha = 0\ . \tag{2.5}$$

Substituting (2.1)—(2.3) into (2.5), we obtain

$$\frac{d}{d\rho}(W+V-U) = -\frac{4}{\rho}V - 2(W+V)\frac{du}{d\rho}\ , \tag{2.6}$$

which is simply (2.4) times $d\sigma/d\rho$. These equations can be readily derived by using either

$$\left[\frac{\delta L}{\delta u}\right]_\omega = \left[\frac{\delta L}{\delta \bar{v}}\right]_\omega = \left[\frac{\delta L}{\delta \sigma}\right]_\omega = 0 \tag{2.7}$$

at a constant ω, or

$$\left[\frac{\delta E}{\delta u}\right]_N = \left[\frac{\delta E}{\delta \bar{v}}\right]_N = \left[\frac{\delta E}{\delta \sigma}\right]_N = 0 \tag{2.8}$$

at a constant N, where E and L are given by (1.39) and (1.40).

In the isotropic coordinates (t,r,α,β), it is useful to introduce

$$x \equiv \dot{u} \equiv ru'\ ,$$
$$y \equiv 1+\dot{v} \equiv 1+rv' = e^{-\bar{v}}\ , \tag{2.9}$$
$$\dot{x} \equiv rx'\ ,\quad \dot{y} \equiv ry'\ ,$$

where, as before

$$u' = du/dr,\quad v' = dv/dr\ ,$$
$$u'' = d^2u/dr^2,\quad v'' = d^2v/dr^2\ , \tag{2.10}$$
$$x' = dx/dr,\quad y' = dy/dr\ .$$

Hence, (2.1)—(2.3) become

$$2\dot{y} + y^2 - 1 = -8\pi G r^2 e^{2v}(W+V+U)\ , \tag{2.11}$$
$$2xy + y^2 - 1 = 8\pi G r^2 e^{2v}(W+V-U)\ , \tag{2.12}$$
$$\dot{x} + \dot{y} + x^2 = 8\pi G r^2 e^{2v}(W-V-U)\ , \tag{2.13}$$

or, alternatively,

$$2v'' + v'^2 + \frac{4}{r}v' = -8\pi G e^{2v}(W+V+U)\ , \tag{2.11'}$$
$$2u'v' + v'^2 + \frac{2}{r}(u'+v') = 8\pi G e^{2v}(W+V-U)\ , \tag{2.12'}$$
$$u'' + v'' + u'^2 + \frac{1}{r}(u'+v') = 8\pi G e^{2v}(W-V-U)\ , \tag{2.13'}$$

and (2.4) can be written as

$$e^{-2v}\left[\sigma'' + \left[u'+v'+\frac{2}{r}\right]\sigma'\right] + \omega^2 e^{-2u}\sigma - \frac{dU}{d\sigma} = 0 \tag{2.14}$$

with $\sigma' = d\sigma/dr$ and $\sigma'' = d^2\sigma/dr^2$.

Substitute these solutions into the integrals (1.22) and (1.22') and (1.32) for $L(g)$ and $L(m)$. Regarding $L = L(g)+L(m)$ as a function of ω, we have

$$\frac{dL}{d\omega} = \left[\frac{\partial L}{\partial \omega}\right]_{u,v,\sigma} = N\ . \tag{2.15}$$

Likewise, we may use these solutions to evaluate the corresponding $E(g)$ and $E(m)$. By regarding the soliton mass

$$M \equiv E = E(g) + E(m) \tag{2.16}$$

as a function of the particle number N, we have, on account of $E = N\omega - L$,

$$\frac{dM}{dN} = \left[\frac{\partial E}{\partial N}\right]_{u,v,\sigma} = \omega \ . \tag{2.17}$$

Set $\omega < m$, and take the regular solutions that satisfy the boundary condition: $\sigma, u, v, \bar{v}$ all $= 0$ at $\rho = \infty$. It follows from (2.14) that $\sigma \to 0$ exponentially at infinity, as indicated by (1.42); likewise, U, V, and W all $\to 0$ exponentially at ∞. Expand u and $\bar{v}$ in powers of ρ^{-1}; since the right-hand sides of (2.1)–(2.3) are all $O(e^{-k\rho})$ where $k = (m^2 - \omega^2)^{1/2}$, so must their left-hand sides be. Thus, to each power of ρ^{-1}, u and $\bar{v}$ must be equal to the Schwarzschild solution; i.e., (1.43) is also accurate to $O(e^{-k\rho})$. The same holds for u and v, as expressed by (1.44).

B. Soliton mass

The soliton mass M is defined by (2.16). As is well known,[4] the same M can also be derived by using the asymptotic behavior of the metric $g_{\rho\rho} = e^{2\bar{v}}$ or $g_{tt} = -e^{2u}$ at $\rho = \infty$:

$$M = \lim_{\rho \to \infty} \rho \bar{v} / G \tag{2.18}$$

or

$$M = -\lim_{\rho \to \infty} \rho u / G \ . \tag{2.19}$$

These formulas can be established by using (2.1); we find

$$\frac{d}{d\rho}[\rho e^{u}(1 - e^{-\bar{v}})] = G \frac{d}{d\rho}[E(g) + E(m)] \ , \tag{2.20}$$

where, because of (1.22) and (1.38),

$$\frac{d}{d\rho}E(g) \equiv (2G)^{-1} e^{u} \left[-e^{\bar{v}} + 2 \left[1 + \rho \frac{du}{d\rho} \right] - e^{-\bar{v}} \left[1 + 2\rho \frac{du}{d\rho} \right] \right]$$

and

$$\frac{d}{d\rho}E(m) \equiv 4\pi \rho^2 e^{u + \bar{v}} (W + V + U) \ .$$

The integration of (2.20) gives (2.18) and (2.19) directly; hence, the constant in the Schwarzschild solution (1.43) is related to $M = E(g) + E(m)$.

There are many alternative formulas for M: (2.1) and (2.11′) can also be written as

$$\frac{d}{d\rho}[\rho(1 - e^{-2\bar{v}})] = 8\pi G \rho^2 (W + V + U) \tag{2.21}$$

and

$$\frac{d}{dr}\left[e^{v/2} r^2 \frac{dv}{dr} \right] = -4\pi G r^2 e^{5v/2} (W + V + U) \ . \tag{2.22}$$

Upon integration and using the Schwarzschild solution at ∞, we obtain

$$M = 4\pi \int_0^\infty (W + V + U) \rho^2 d\rho \tag{2.23}$$

and

$$M = 4\pi \int_0^\infty (W + V + U) e^{5v/2} r^2 dr \ . \tag{2.24}$$

Either expression establishes the positivity of M. In addition, from (2.21) and $\bar{v} = 0$ at ∞, it follows that

$$0 \le y = e^{-\bar{v}} \le 1 \ . \tag{2.25}$$

By taking the combination $G_\alpha{}^\alpha + \frac{1}{2}(G_\rho{}^\rho - G_t{}^t)$, we have

$$\frac{d}{d\rho}\left[\rho^2 e^{u - \bar{v}} \frac{du}{d\rho} \right] = 8\pi G \rho^2 e^{u + \bar{v}} (2W - U) \ , \tag{2.26}$$

which leads to still another formula for M:

$$M = 8\pi \int_0^\infty (2W - U) e^{u + \bar{v}} \rho^2 d\rho = 8\pi \int_0^\infty (2W - U) e^{u + 3v} r^2 dr \ . \tag{2.27}$$

This may be written as the virial theorem

$$E(g) + 4\pi \int (-3W + V + 3U) e^{u + \bar{v}} \rho^2 d\rho = 0 \ .$$

The same result can also be derived by making a scale transformation changing $\rho, u(\rho), \bar{v}(\rho), \sigma(\rho)$ to $\lambda\rho, u(\lambda\rho), \bar{v}(\lambda\rho), \sigma(\lambda\rho)$ in (1.22), (1.37), and (1.38), and then setting $(\partial E / \partial \lambda)_N = 0$.

Another relation can be obtained by considering the difference $G_\rho{}^\rho - G_t{}^t$; this gives

$$\frac{d}{d\rho}(u + \bar{v}) = 8\pi G \rho e^{2\bar{v}} (W + V) \tag{2.28}$$

and is always positive. Because $u + \bar{v} = 0$ at ∞,

$$u + \bar{v} < 0 \tag{2.29}$$

at all finite ρ.

C. Behavior near the origin

From (2.1), (2.2), and (2.4), we see that as $\rho \to 0$,

$$\begin{aligned} u &= u(0) + O(\rho^2) \ , \\ \bar{v} &= O(\rho^2) \ , \end{aligned} \tag{2.30}$$

and

$$\sigma = \sigma(0) + O(\rho^2) \ .$$

These imply that in the isotropic coordinates, as $r \to 0$ the variables x and y, defined by (2.9), are of the form

$$\begin{aligned} x &= \tfrac{1}{2} a r^2 + O(r^4) \\ \text{and} \qquad & \qquad (2.31) \\ y &= 1 + \tfrac{1}{2} b r^2 + O(r^4) \ , \end{aligned}$$

where a and b are constants. By using (2.11)–(2.13), we find

$$\left[\frac{dx}{dy}\right]_0 \equiv \frac{a}{b} = \frac{2U(0)-4W(0)}{U(0)+W(0)} \geq -4 , \tag{2.32}$$

where $U(0)$ and $W(0)$ are the values of U and W at $r=0$. [Note that $V(0)=0$ because of (2.30).]

D. Integration method

It is convenient to introduce

$$e^{-\bar{u}(\rho)} \equiv \frac{\omega}{m} e^{-u(\rho)} . \tag{2.33}$$

Because $d\bar{u}/d\rho = du/d\rho$ and

$$W = \tfrac{1}{2} m^2 e^{-2\bar{u}} \sigma^2 , \tag{2.34}$$

when expressed in terms of $\bar{u}$, $\bar{v}$, and σ, the basic equations (2.1)—(2.4) do not contain ω explicitly. We may use the boundary condition (2.30) to integrate (2.1), (2.2), and (2.4) from $\rho=0$ outwards. Fix

$$e^{-\bar{u}(0)} \equiv \frac{\omega}{m} e^{-u(0)} \tag{2.35}$$

and adjust $\sigma(0)$ so that $\sigma(\rho) \to 0$ at ∞, after a given number n of nodes; ω is then determined by

$$\frac{\omega}{m} = e^{-\bar{u}(\infty)} . \tag{2.36}$$

E. W-dominating region

When the initial value $e^{-\bar{u}(0)}$ is increased steadily, among the three matter-energy terms W, V, and U, W becomes more and more important (at least near the origin). Whenever that happens, there is an important simplification.

Setting in (2.11)—(2.13)

$$V = U = 0 , \tag{2.37}$$

we find

$$\dot{y} = 1 - xy - y^2 , \tag{2.38}$$

$$\dot{x} = -2 - x^2 + 3xy + 2y^2 , \tag{2.39}$$

and

$$\frac{dy}{dx} = \frac{1 - xy - y^2}{-2 - x^2 + 3xy + 2y^2} . \tag{2.40}$$

It is convenient to think of

$$\tau \equiv \ln r \tag{2.41}$$

as a fictitious time, and $x(\tau), y(\tau)$ as the trajectory of a "particle." There are two critical points, defined by $\dot{x} = \dot{y} = 0$:

$$\text{(i) } x = 0 \text{ and } y = 1 \tag{2.42}$$

and

$$\text{(ii) } x = y = 2^{-1/2} . \tag{2.43}$$

Assuming W dominance, we find that when $\tau = -\infty$ (i.e., $r=0$) the trajectory must start from (i) with an initial slope

$$\left[\frac{dy}{dx}\right]_0 = -\frac{1}{4} , \tag{2.44}$$

in accordance with (2.31), (2.32), and (2.37). Equation (2.40) then determines a universal curve, which terminates at (ii), as given by the solid curve in Figs. 3(a) and 3(b). There is a curious spiral structure near the end point (ii). Since the W-dominating region plays a more important role for the regular soliton stars, we shall postpone the detailed discussion of this spiral trajectory to a later paper.[5]

The Schwarschild solution corresponds to the hyperbola

$$2xy + y^2 - 1 = 0 , \tag{2.45}$$

indicated by the dashed line in Fig. 3(a); it also satisfies (2.40).

For the actual solution of (2.1)—(2.4), its (x,y) trajectory always starts (at $r=0$) at point (i) with a slope $\leq -\frac{1}{4}$. When the initial value $e^{-\bar{u}(0)}$ is large, W dominance is a good approximation at small r; the corresponding trajectory in the (x,y) plane follows fairly closely the universal (W-dominating) curve. As r increases, W no longer dominates. The trajectory gradually changes its course and finally approaches the Schwarzschild hyperbola (2.45) and returns to point (i) as $r \to \infty$, but at a slope $dy/dx = -1$.

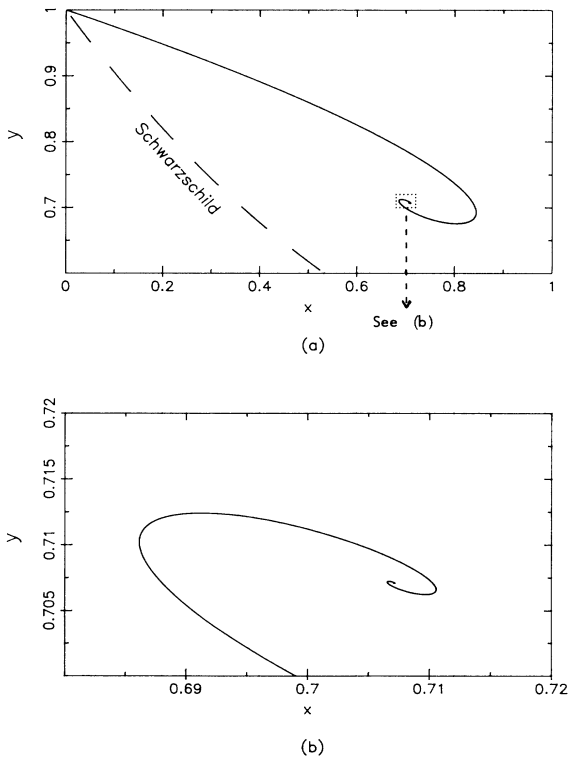

FIG. 3. The solid curve is the universal (W-dominating) trajectory defined by (2.40) and (2.44). The dashed curve is the Schwarzschild hyperbola $2xy + y^2 - 1 = 0$.

III. NEWTONIAN LIMIT

For the Newtonian limit, it is more convenient to adopt the isotropic coordinates (t,r,α,β). We assume, as in (1.33),

$$\phi=2^{-1/2}\sigma(r)e^{-i\omega t} \tag{3.1}$$

but with ω only slightly less than m, so that

$$\xi\equiv\left[1-\frac{\omega^2}{m^2}\right]^{1/2}\ll 1\ ; \tag{3.2}$$

in addition, the matter density is supposed to be relatively low (proportional to ξ^2, as we shall see). Hence, we neglect the nonlinear σ coupling and set, instead of (1.34),

$$U=\tfrac{1}{2}m^2\sigma^2\ . \tag{3.3}$$

The other energy densities V and W remain given by (1.35) and (1.36). The deviations of the metric e^{2u} and e^{2v} from 1 are also small, by definition of the Newtonian limit; i.e.,

$$|u|\ \text{ and }\ |v|\ll 1\ . \tag{3.4}$$

Neglecting u^2 and v^2, (2.11′)–(2.13′) become

$$2v''+\frac{4}{r}v'=-8\pi G(W+V+U)\ , \tag{3.5}$$

$$\frac{2}{r}(u'+v')=8\pi G(W+V-U)\ , \tag{3.6}$$

and

$$u''+v''+\frac{1}{r}(u'+v')=8\pi G(W-V-U)\ . \tag{3.7}$$

For $\omega<m$, σ decreases with increasing r. Approximately, σ is proportional to

$$\exp[-(m^2-\omega^2)^{1/2}r]=e^{-\xi mr}\ . \tag{3.8}$$

Thus, a typical r derivative d/dr brings a factor ξm; i.e.,

$$\frac{d}{dr}\sim\xi m \tag{3.9}$$

and therefore we may estimate

$$\frac{\sigma'}{m\sigma}=O(\xi)\ . \tag{3.10}$$

For the same reason, $V=\frac{1}{2}e^{-2v}\sigma'^2$ is small compared to U by a factor $\sim\xi^2$. Since ω is near m, $W=\frac{1}{2}\omega^2e^{-2u}\sigma^2$ differs from U by a similarly small factor; i.e.,

$$\frac{V}{U}=O(\xi^2)\ \text{ and }\ \frac{U-W}{U}=O(\xi^2)\ . \tag{3.11}$$

In the isotropic coordinates, (2.6) takes on the form (without approximation)

$$U'-V'-W'=2\left[u'+v'+\frac{2}{r}\right]V+2u'W\ . \tag{3.12}$$

Because of (3.8), the radial size of the mini-soliton star is $\sim(\xi m)^{-1}$; hence, for the greater part of the solution

$$r\sim(\xi m)^{-1}\ . \tag{3.13}$$

Substituting (3.4), (3.9), (3.11), and (3.13) into (3.12), we see that $u'W$ is of the same order as V'; since $W\sim U\sim V/\xi^2$, we find

$$u=O(\xi^2)\ . \tag{3.14}$$

From (3.5), we estimate

$$v=O(GU/\xi^2m^2)\ ,$$

and from (3.6), or (3.7),

$$u+v=O(GU/m^2)\ .$$

Therefore,

$$GU/m^2=O(\xi^4)\ , \tag{3.15}$$

$$v=O(\xi^2)\ , \tag{3.16}$$

and

$$u+v=O(\xi^4)\ . \tag{3.17}$$

Substituting (3.3) into (2.14) and using (3.16) and (3.17), we derive, accurate up to $O(\xi^2m^2\sigma)$,

$$\sigma''+\frac{2}{r}\sigma'=(m^2-\omega^2e^{-2u})\sigma\ . \tag{3.18}$$

Likewise, because of (3.3), (3.9), (3.11), and (3.17), we can reduce (3.5) into

$$u''+\frac{2}{r}u'=4\pi Gm^2\sigma^2\ , \tag{3.19}$$

which is accurate up to $O(\xi^4m^2)$. Define

$$\gamma\equiv 1-\frac{\omega^2}{m^2}e^{-2u}\ . \tag{3.20}$$

Equations (3.18) and (3.19) can be written as

$$\nabla^2\sigma=\gamma m^2\sigma \tag{3.21}$$

and

$$\nabla^2\gamma=8\pi G\omega^2\sigma^2\ , \tag{3.22}$$

where $\nabla^2=(d^2/dr^2)-2r^{-1}(d/dr)$. These equations can also be derived directly by using the Newtonian gravity.

Introducing

$$\gamma=\lambda^2\hat{\gamma},\quad r=(m\lambda)^{-1}\hat{r}\ ,$$
$$\sigma=(8\pi G)^{-1/2}(m/\omega)\lambda^2\hat{\sigma}\ , \tag{3.23}$$
$$\hat{\nabla}^2\equiv\frac{d^2}{d\hat{r}^2}-\frac{2}{\hat{r}}\frac{d}{d\hat{r}}\ ,$$

we convert (3.21) and (3.22) into a set of scale-independent equations

$$\hat{\nabla}^2\hat{\sigma}=\hat{\gamma}\,\hat{\sigma} \tag{3.24}$$

and

$$\hat{\nabla}^2\hat{\gamma}=\hat{\sigma}^2\ . \tag{3.25}$$

The solution of $\hat{\sigma}(\hat{r})$ can be characterized by its number of nodes n. The ground state corresponds to $n=0$. It is convenient to fix (for any n)

$$\hat{\sigma}=1 \text{ at } \hat{r}=0 . \tag{3.26}$$

These solutions are then universal functions. The special cases $n=0$ and 5 are given in Fig. 4 as examples.

Take the solution for the ground state, $n=0$. From the numerical result, we find

$$\hat{\gamma}\to\hat{\gamma}_0=-0.918\,58 \text{ as } \hat{r}\to 0 , \tag{3.27}$$

and

$$\hat{\gamma}\to\hat{\gamma}_\infty-(\hat{\gamma}_1/\hat{r}) \text{ as } \hat{r}\to\infty ,$$

where

$$\hat{\gamma}_\infty=0.978\,96 \text{ and } \hat{\gamma}_1=3.468\,26 . \tag{3.28}$$

The asymptotic behavior of the matter field $\hat{\sigma}$ is given by

$$\hat{\sigma}\to\hat{\sigma}_\infty e^{-\hat{\gamma}_\infty^{1/2}\hat{r}}\hat{r}^{\nu} \text{ as } \hat{r}\to\infty ,$$

where

$$\hat{\sigma}_\infty=3.3943 \text{ and } 2(\nu+1)=\hat{\gamma}_1/\hat{\gamma}_\infty . \tag{3.29}$$

Once $\hat{\gamma}$ and $\hat{\sigma}$ are known, γ and σ can be obtained from (3.23), in which λ^2 is related to ω/m by taking the $r=\infty$ limit of the first equation, $\gamma=\lambda^2\hat{\gamma}$. We have

$$\xi^2=1-\frac{\omega^2}{m^2}=\lambda^2\hat{\gamma}_\infty . \tag{3.30}$$

Neglecting ξ^4,

$$u=-v=\tfrac{1}{2}\lambda^2(\hat{\gamma}-\hat{\gamma}_\infty) . \tag{3.31}$$

The particle number is

$$N=4\pi\int_0^\infty \omega\sigma^2 e^{u+3v}r^2dr$$
$$\simeq(2Gm^2)^{-1}\lambda\int\hat{\sigma}^2\hat{r}^2d\hat{r}$$

where the integral is related to the asymptotic behavior (3.28) of $\hat{\gamma}$, through Gauss's theorem. We find

$$N=(2Gm^2)^{-1}\hat{\gamma}_\infty^{-1/2}\hat{\gamma}_1\left[1-\frac{\omega^2}{m^2}\right]^{1/2} . \tag{3.32}$$

Let

$$\omega=m(1-\epsilon) . \tag{3.33}$$

For ϵ small, (3.32) becomes

$$N=N_0\epsilon^{1/2} , \tag{3.34}$$

where

$$N_0=(2Gm^2)^{-1}(2/\hat{\gamma}_\infty)^{1/2}\hat{\gamma}_1 . \tag{3.35}$$

Because of (2.17) and (3.33),

$$\frac{dM}{dN}=m(1-\epsilon)=m\left[1-\left[\frac{N}{N_0}\right]^2\right] , \tag{3.36}$$

which gives

$$M=Nm(1-\tfrac{1}{3}\epsilon) . \tag{3.37}$$

The values of $\hat{\gamma}_0$, $\hat{\gamma}_\infty$, and $\hat{\gamma}_1$ for $n=0,1,\ldots,5$ are given in Table I.

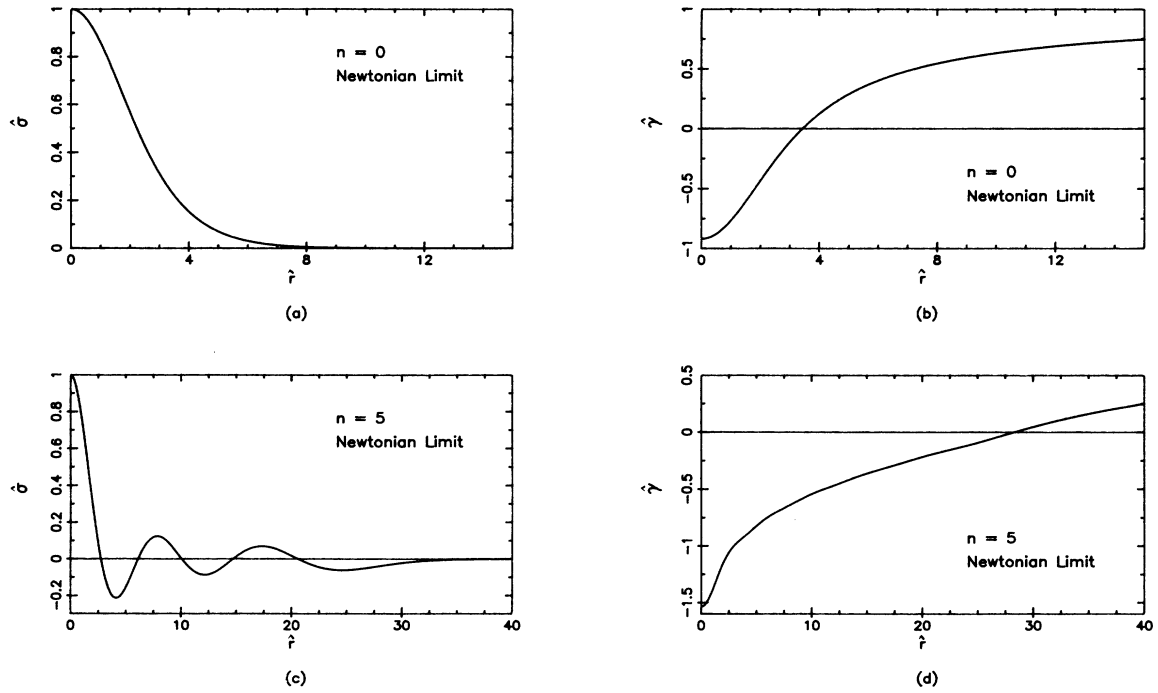

FIG. 4. Newtonian limit of the gravitational potential and the matter amplitude when the number of nodes $n=0$ and 5. See (3.23)—(3.26) for the definitions of $\hat{\gamma}$ and $\hat{\sigma}$.

TABLE I. Values of $\hat{\gamma}_0$, $\hat{\gamma}_\infty$, and $\hat{\gamma}_1$ for the Newtonian solutions when the number of nodes $n=0,1,\ldots,5$. [See (3.27)–(3.28) for their definitions.]

n	$\hat{\gamma}_0$	$\hat{\gamma}_\infty$	$\hat{\gamma}_1$
0	−0.918 58	0.978 96	3.468 26
1	−1.209 96	0.916 27	7.713 95
2	−1.343 70	0.892 21	11.935 47
3	−1.428 28	0.877 99	16.132 18
4	−1.489 43	0.868 12	20.310 19
5	−1.537 01	0.860 66	24.473 66

IV. NUMERICAL SOLUTIONS

We have made extensive numerical studies for the exact equations (2.1)–(2.4) when

$$U=\tfrac{1}{2}m^2\sigma^2 . \tag{4.1}$$

In spite of the simplicity of the basic theory, the result is surprisingly nontrivial. In this case, the matter equation (2.4) becomes linear in σ, and all matter energy densities U,V,W are quadratic in σ. Define

$$\begin{aligned}&\bar{\rho}\equiv m\rho,\quad \bar{\sigma}\equiv(16\pi G)^{1/2}\sigma ,\\ &\bar{U}\equiv\tfrac{1}{2}\bar{\sigma}^2,\quad \bar{V}\equiv\tfrac{1}{2}e^{-2\bar{v}}(d\bar{\sigma}/d\bar{\rho})^2 ,\\ &\bar{W}\equiv\tfrac{1}{2}e^{-2\bar{u}}\bar{\sigma}^2 ,\end{aligned} \tag{4.2}$$

where $e^{-\bar{u}}$ is given by (2.33):

$$e^{-\bar{u}}=\frac{\omega}{m}e^{-u} . \tag{4.3}$$

Equations (2.1), (2.2), and (2.4) can be reduced to

$$e^{-2\bar{v}}-1-2\bar{\rho}e^{-2\bar{v}}(d\bar{v}/d\bar{\rho})=-\tfrac{1}{2}(\bar{W}+\bar{V}+\bar{U})\bar{\rho}^2 , \tag{4.4}$$

$$e^{-2\bar{v}}-1+2\bar{\rho}e^{-2\bar{v}}(d\bar{u}/d\bar{\rho})=\tfrac{1}{2}(\bar{W}+\bar{V}-\bar{U})\bar{\rho}^2 , \tag{4.5}$$

and

$$e^{-2\bar{v}}\{(d^2\bar{\sigma}/d\bar{\rho}^2)+(d\bar{\sigma}/d\bar{\rho})[(2/\bar{\rho})+(d/d\bar{\rho})(\bar{u}-\bar{v})]\}=(1-e^{-2\bar{u}})\bar{\sigma} , \tag{4.6}$$

in which both dimensions m and G have been scaled away. [Likewise, (2.3) can also be reduced, since it is derivable from (4.4)–(4.6).]

We then apply the integration method outlined in Sec. II D to (4.4)–(4.6). At each radial point, these numerical solutions carry an accuracy of about one part in 10^8. The main features, which we find to be both complex and illuminating, are given below.

A. M vs N

For a fixed

$$n=\text{number of nodes in } \sigma(r) , \tag{4.7}$$

we first assign an initial value $e^{-\bar{u}(0)}$, defined by (2.35). A solution may then be derived by following the steps given in Sec. II D. This yields a mass M and a particle number N. As illustrated in Fig. 1, when $e^{-\bar{u}(0)}$ increases from 1,

$$M\equiv M_n(N) \tag{4.8}$$

rises from the origin $M=0$ and $N=0$ to its first cusp, labeled $(n,1)$ with

$$M=M(n,1)\ \text{ and }\ N=N(n,1) ; \tag{4.9}$$

then it changes its course abruptly. (*Note added in proof.* It has been brought to our attention that the lowest branch of the $1s$ solution has already been analyzed by R. Ruffini and S. Bonazzola [Phys. Rev. **187**, 1767 (1969)] and by W. Thirring [Phys. Lett. **127B**, 27 (1983)].) As $e^{-\bar{u}(0)}$ keeps on increasing, the curve $M_n(N)$ now descends until it reaches its second cusp, labeled $(n,2)$ with

$$M=M(n,2)\ \text{ and }\ N=N(n,2) ; \tag{4.10}$$

then it turns back and rises again, up to third cusp $(n,3),\ldots$. Each of these cusps is labeled (n,n'), with $n'=1,2,\ldots$ indicating its consecutive order. The curve $M_n(N)$ approaches a limiting point as $e^{-\bar{u}(0)}\to\infty$. (See Secs. IV B and IV D for further discussions.) Everywhere on the curve, we have

$$\frac{dM_n(N)}{dN}=\omega<m . \tag{4.11}$$

Along each such zigzag curve $M_n(N)$, for a given particle number N, quite often, there would be more than one stellar mass M. The minimum value always lies on its first portion between the origin and $(n,1)$, which will be defined to be

$$[M_n(N)]_{\min} . \tag{4.12}$$

Hence, each curve $[M_n(N)]_{\min}$ has a finite length, beginning at the origin and ending at $(n,1)$. At any N, whenever $[M_n(N)]_{\min}$ exists, it satisfies the inequalities

$$[M_n(N)]_{\min}<[M_{n+1}(N)]_{\min}<Nm . \tag{4.13}$$

For example, for $n=0$ the curve $[M_0(N)]_{\min}$ ends at the cusp (0,1), with

$$M(0,1)=0.633(Gm)^{-1}\ ,$$
$$N(0,1)=0.653(Gm^2)^{-1}\ , \tag{4.14}$$

and, at that point, ω is

$$\omega(0,1)=0.853m\ .$$

Within the interval $N<N(0,1)$, we have

$$[M_0(N)]_{\min}<[M_1(N)]_{\min}<[M_2(N)]_{\min}<\cdots\ .$$

But for $N>N(0,1)$, there is no longer any $n=0$ solution. In the range $N(1,1)>N>N(0,1)$, the minimum stellar mass is given by the $n=1$ solution. The curve $[M_1(N)]_{\min}$ terminates at the cusp (1,1) with

$$M(1,1)=1.356(Gm)^{-1}\ ,$$
$$N(1,1)=1.392(Gm^2)^{-1}\ , \tag{4.15}$$

and, at that point, ω is

$$\omega(1,1)=0.881m\ .$$

For $N>N(1,1)$, there is no longer any $n=1$ solution. The $n=2$ solution takes over until $N=N(2,1)$; in turn, $[M_2(n)]_{\min}$ ends abruptly at the cusp (2,1), with

$$M(2,1)=2.085(Gm^2)^{-1}\ ,$$
$$N(2,1)=2.138(Gm^2)^{-1}\ , \tag{4.16}$$

and, at that point, ω is

$$\omega(2,1)=0.888m\ .$$

Further details are given in Table II (in Sec. IV E).

The same pattern repeats itself, as illustrated in Fig. 5(a). In Fig. 5(b) we plot $M(n,1)-mN(n,1)$ vs $N(n,1)$ for $n=0,1,\ldots,10$; these points lie surprisingly well on a straight line:

$$M(n,1)=m(1-0.022\,173)N(n,1)$$
$$-(Gm)^{-1}(5.232\times10^{-3}+\delta) \tag{4.17}$$

with $\delta\sim10^{-4}$ shown in Fig. 5(c). We have also examined the relation between $M(n,1)$ and $N(n,1)$ for much larger n, and find the straight-line fit still good. In Fig. 5(d) we give the plot for n up to 56; the best fit is

$$M(n,1)=m(1-0.021\,576)N(n,1)$$
$$-(Gm)^{-1}(1.8542\times10^{-2}$$
$$-1.3750\times10^{-2}e^{-\alpha Gm^2N}+\epsilon) \tag{4.18}$$

with

$$\alpha=5.81\times10^{-2}\ ,$$

and $\epsilon\sim10^{-5}$ shown in Fig. 6.

From (1.37) and (2.27), we see that

$$M-N\omega=2\int(W-U)\,|g|^{1/2}dx^1dx^2dx^3\ . \tag{4.19}$$

A comparison with (4.14)–(4.16) indicates that its left-hand side is only $\sim10^{-1}$ times M; i.e., $W-U$ is relatively small (compared to U), which is reminiscent of the Newtonian case. This is borne out by comparing the ex-

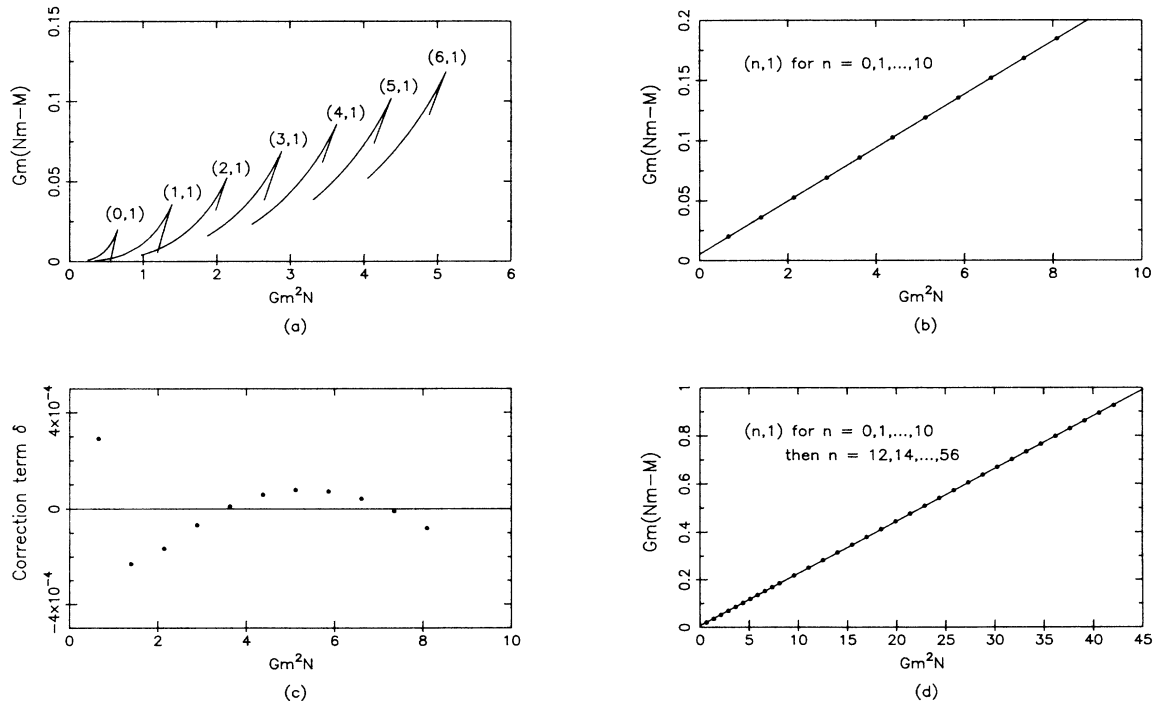

FIG. 5. Binding energy $Nm-M$ vs N for $n=0,1,\ldots,6$ (a), where $(n,1)$ denotes the first cusp when the number of nodes is n. The nearly linear dependence of $M(n,1)$ on $N(n,1)$ is illustrated for n up to 10 in (b) and n up to 56 in (d). The correction term δ, defined in (4.17), for $n=0,1,\ldots,10$ is given in (c).

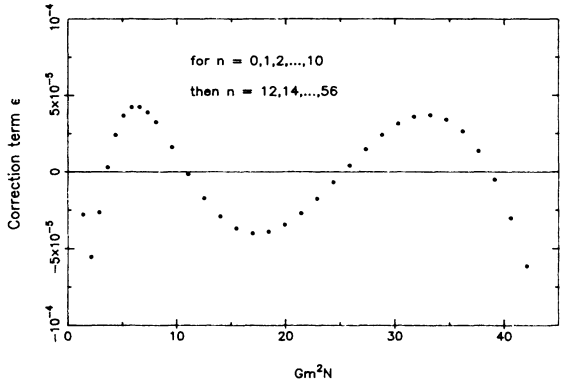

FIG. 6. Correction term ϵ in the mass formula (4.18), for $n=0,1,\ldots,56$.

act solution with the Newtonian solution of the same n and the same particle number $=N(n,1)$. [Note that along $M_n(N)$ during its initial portion, from the origin $M=0,N=0$ to its first cusp $(n,1)$, the initial value $e^{-\bar{u}(0)}$ is still not large; later on, when $e^{-\bar{u}(0)}$ becomes $\gg 1$, the exact solution is quite different from the Newtonian approximation.]

Another simpler comparison can be made by approximating (4.17) as

$$M\simeq m(1-0.022\,173)N$$

and combining it with the Newtonian formula (3.37); this leads to setting

$$\tfrac{1}{3}\epsilon=0.022\,173$$

in (3.34) and (3.35), from which a Newtonian approximation of $N=N(n,1)$ can be derived. By using Table I, we find $N(n,1)$ times $(Gm^2)^{-1}$ calculated from the Newtonian formulas (3.34) and (3.35), to be 0.64 for $n=0$, 1.50 for $n=1$, 2.30 for $n=2$, 3.14 for $n=3$, 3.97 for $n=4$, and 4.81 for $n=5$. As can be seen from Fig. 5(b) and (4.14)—(4.16), the Newtonian approximations are within 10% of the exact values.

At first sight, this seems extraordinary. The Newtonian curve $M=M_n(N)$, for any n, has *no* cusp. How can the exact solution at its cusp resemble even remotely the Newtonian solution? As will be discussed in the next section, the appearance of cusps, though dramatic, depends on the second derivative $d^2L/d\omega^2$. Hence, it is sensitive to small differences between solutions.

B. Cusps

Using the exact solution and keeping n, the number of nodes in σ, fixed, we may determine the total Lagrangian from (4.19):

$$L=L_n(\omega)\equiv 2\int (U-W)\,|g|^{1/2}dx^1dx^2dx^3\ . \tag{4.20}$$

The mass function $M_n(N)$ is related to $L_n(\omega)$ by

$$M_n(N)=N\omega-L_n(\omega)\ , \tag{4.21}$$

where

$$N=\frac{d}{d\omega}L_n(\omega)$$

and

$$\omega=\frac{d}{dN}M_n(N)\ , \tag{4.22}$$

in accordance with (2.15)—(2.17). Hence the slope of $M_n(N)$ is always positive, and $<m$. It has a cusp at

$$\frac{dN}{d\omega}=\frac{d^2L_n(\omega)}{d\omega^2}=0\ , \tag{4.23}$$

since $dN/d\omega$ changes sign whenever ω passes its cusp value $\omega(n,n')$.

As mentioned before, for each initial value $e^{-\bar{u}(0)}>1$, we determine a solution; ω is related to $\bar{u}$ at ∞ through (2.36):

$$\omega=me^{-\bar{u}(\infty)}\ . \tag{4.24}$$

The relation between $\bar{u}(0)$ and $\bar{u}(\infty)$ is complicated. From (2.28) and $\bar{v}(0)=\bar{v}(\infty)=0$, we see that

$$\bar{u}(\infty)-\bar{u}(0)=\int_0^\infty 8\pi G\rho e^{2\bar{v}}(W+V)d\rho\ ;$$

consequently,

$$\ln\omega/m=-\bar{u}(0)-\int_0^\infty 8\pi G\rho e^{2\bar{v}}(W+V)d\rho\ . \tag{4.25}$$

Now $-\bar{u}(0)$ is >0, (4.25) gives $\ln\omega/m$ as the difference between two positive numbers, which can both be quite large, especially when $e^{-\bar{u}(0)}$ is $\gg 1$. For any given n, ω turns out to be an oscillatory function of $e^{-\bar{u}(0)}$, beginning at m when $-\bar{u}(0)=0$ and approaching a constant as $-\bar{u}(0)\to\infty$. In Figs. 7(a) and 7(b) we give two examples of ω vs $-\bar{u}(0)$ for $n=0$ and 10. Along each curve, label the consecutive minima and maxima as $a_n,b_n,c_n,\ldots$ [in the direction of increasing $-\bar{u}(0)$] as shown in Figs. 7(a) and 7(b). At each $a_n,b_n,c_n,\ldots$, we have

$$\frac{d\omega}{d\bar{u}(0)}=0\ . \tag{4.26}$$

Likewise, as shown in Figs. 8(a) and 8(b), for any given n, N is also an oscillatory function of the initial value $e^{-\bar{u}(0)}$; the cusps $(n,1),(n,2),\ldots$ are precisely its consecutive maxima and minima. Furthermore, each (n,n') cusp (when n' varies from 1 to 2,3,...) must be sandwiched between a maximum and a minimum of the ω vs $e^{-\bar{u}(0)}$ curve. This is because at each of the extremities $a_n,b_n,c_n,\ldots$, we have (4.26); therefore, $d\bar{u}(0)/d\omega=\infty$ and

$$\frac{dN}{d\omega}=\frac{dN}{d\bar{u}(0)}\frac{d\bar{u}(0)}{d\omega}=\infty\ . \tag{4.27}$$

As can be seen from Figs. 8(c) and 8(d), along the N vs ω curve (keeping n fixed and moving in the direction of increasing $e^{-\bar{u}(0)}$), one encounters first the cusp $(n,1)$, then a_n, after that the cusp $(n,2)$, then b_n, then $(n,3)$, then c_n, etc. For very large $e^{-\bar{u}(0)}$, although the curves M vs N, N vs ω, and ω vs $e^{-\bar{u}(0)}$ all keep on oscillating, the values of M, N, and ω hardly deviate at all from their asymptotic limits.

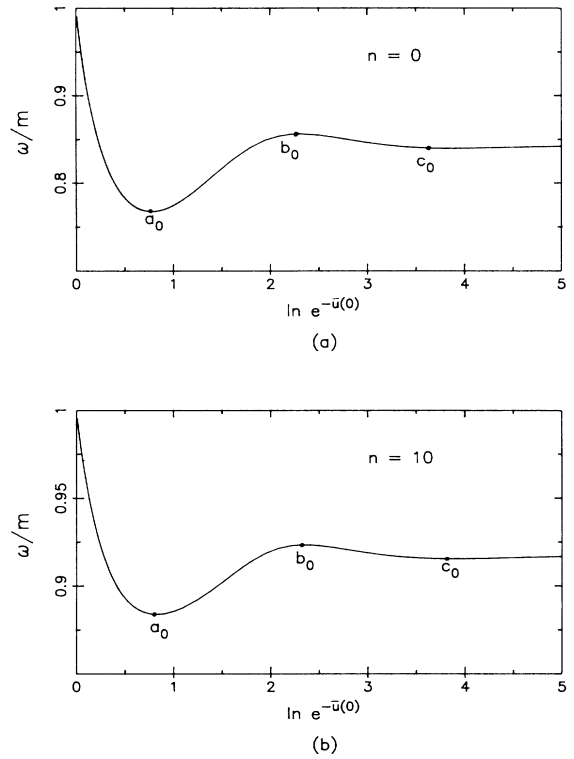

FIG. 7. Frequency ω vs the initial value $\ln e^{-\bar{u}(0)}$ for $n=0$ and 10; the consecutive minima and maxima are denoted by $a_n, b_n, c_n, \ldots$.

C. (x,y) trajectories

For any given n, each initial value $e^{-\bar{u}(0)} \geq 1$ determines a solution, from which a trajectory in the (x,y) plane can be determined, where x and y are defined by (2.9). When $\rho \to 0$, the trajectory starts at

$$x=0 \quad \text{and} \quad y=1 \tag{4.28}$$

with an initial slope, according to (2.32)—(2.35),

$$-\left[\frac{dy}{dx}\right]_0 = \frac{e^{-2\bar{u}(0)}+1}{4e^{-2\bar{u}(0)}-2} \, . \tag{4.29}$$

Hence

$$1 \geq -\left[\frac{dy}{dx}\right]_0 \geq \frac{1}{4} \, . \tag{4.30}$$

Each trajectory traces at least one loop, since as $\rho \to \infty$, it has to return to the same point (4.28) with a slope

$$-\left[\frac{dy}{dx}\right]_\infty = 1 \, ; \tag{4.31}$$

thereby, it also approaches the hyperbola, determined from the Schwarzschild solution,

$$2xy + y^2 - 1 = 0 \, . \tag{4.32}$$

For small $-\bar{u}(0)$, the trajectory stays fairly close to the Schwarzschild hyperbola, as can be seen by using the Newtonian solution. When $-\bar{u}(0)$ becomes large, there

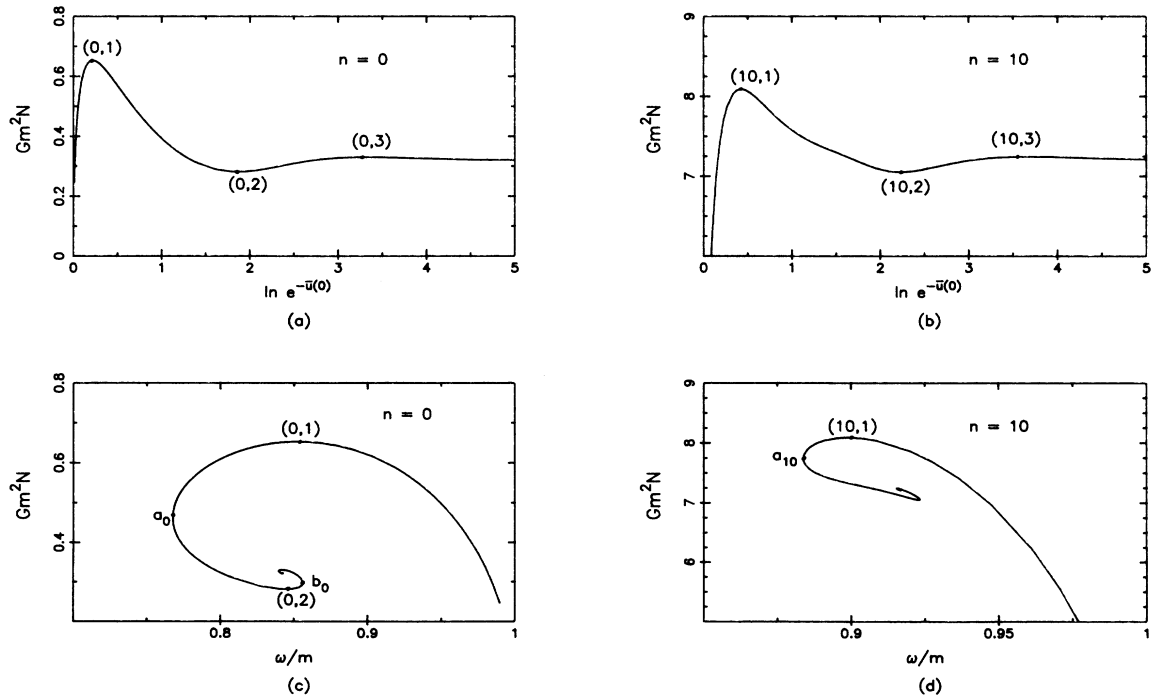

FIG. 8. Particle number N vs the initial value $\ln e^{-\bar{u}(0)}$ (a) and (b) and vs the frequency ω (c) and (d) for $n=0$ and 10. Note $dN/d\omega=0$ at $(n,1),(n,2),\ldots$, but ∞ at $a_n, b_n, \ldots$; this explains the consecutive order of $(n,1), a_n, (n,2), b_n, (n,3), c_n, \ldots$ on the N vs ω curves.

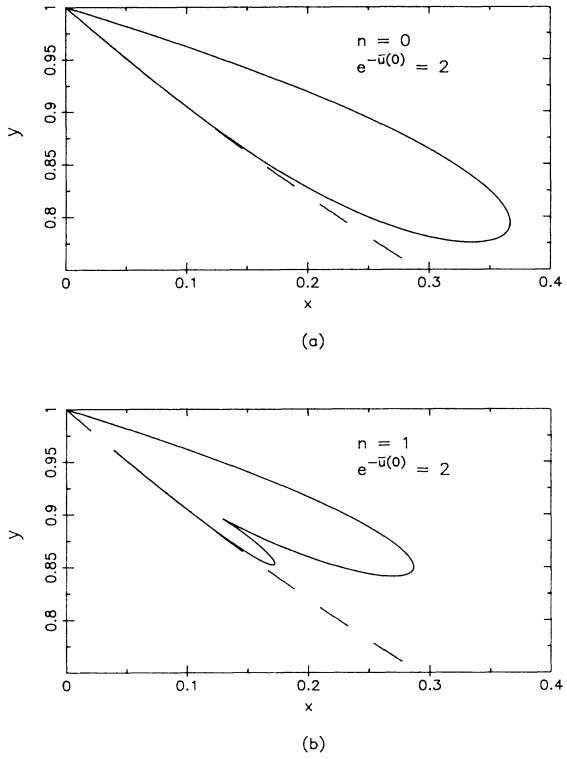

FIG. 9. The (x,y) trajectory of the solution with an initial value $e^{-\bar{u}(0)}=2$. (a) is for $n=0$ and (b) for $n=1$. The dashed curve is the Schwarzschild hyperbola $2xy+y^2-1=0$.

appear several interesting features.

As examples, we give the (x,y) trajectories for $n=0$ and 1 in Fig. 9, $n=10$ in Fig. 10(d), all for the initial value

$$e^{-\bar{u}(0)}=2\ . \tag{4.33}$$

The Schwarzschild hyperbola is always represented by the dashed curves in these figures.

From Fig. 9(a), for $n=0$, we see that as ρ increases, the (x,y) trajectory starts from $(x=0,y=1)$ and ends at the same point, making a single loop. For $n=1$ in Fig. 9(b), it makes one extra loop at about the middle; for $n=10$ in Fig. 10(d), it makes ten more loops. These are to be expected, because at each σ node by definition $\sigma=0$, and therefore U and W are also zero. Because U and W are positive functions, these must be their minima. The oscillations of U and W induce a similar behavior in both x and y, on account of (2.11)–(2.13), which produces these loops in the (x,y) trajectories. Further illustrations of σ, x, and y vs ρ are given in Figs. 10(a)–10(c), for $n=10$.

D. Solutions when $e^{-\bar{u}(0)}\gg 1$

At the origin $\rho=0$, we have $V=0$ because of (2.32), and $W\gg U$ since

$$\frac{W}{U}=e^{-2\bar{u}}$$

and $e^{-\bar{u}(0)}$ is assumed to be $\gg 1$. Hence, the W-dominating trajectory of Fig. 3 becomes applicable in the central part of the soliton. In Figs. 11 and 12 we give the

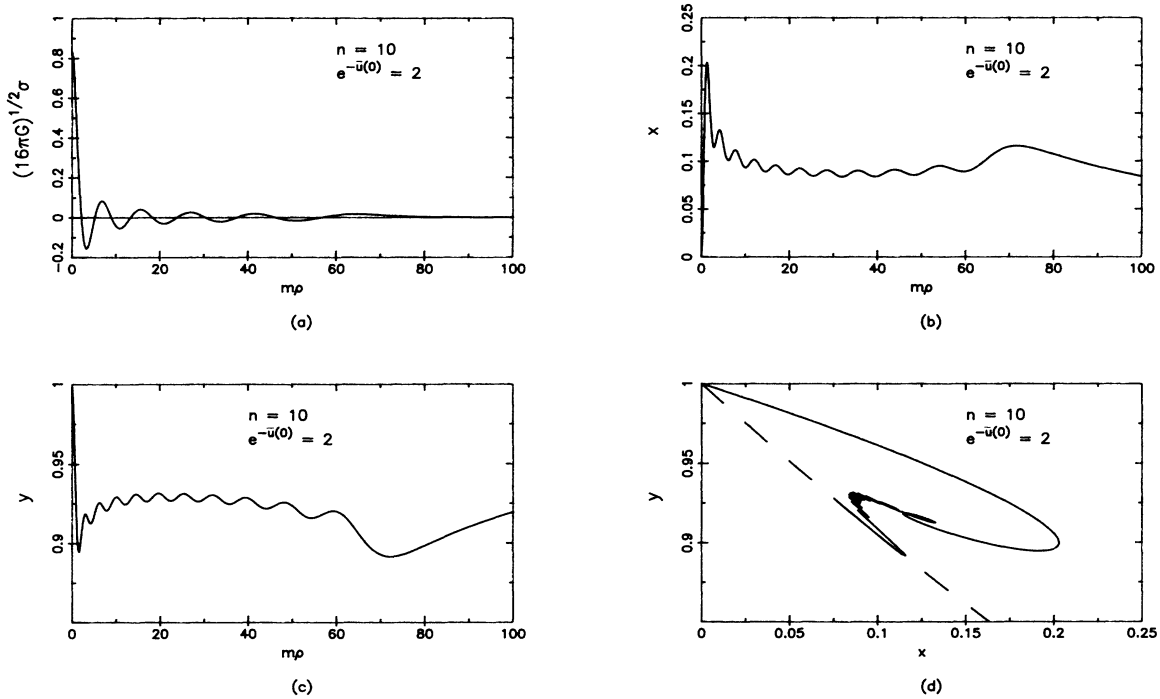

FIG. 10. Solution for a mini-soliton star with ten nodes ($n=10$) and an initial value $e^{-\bar{u}(0)}=2$. (a)–(c) give σ, x, and y vs the radius ρ. (d) shows its (x,y) trajectory, which makes ten extra loops before approaching the Schwarzschild hyperbola $2xy+y^2-1$ (dashed curve) as $\rho\to\infty$.

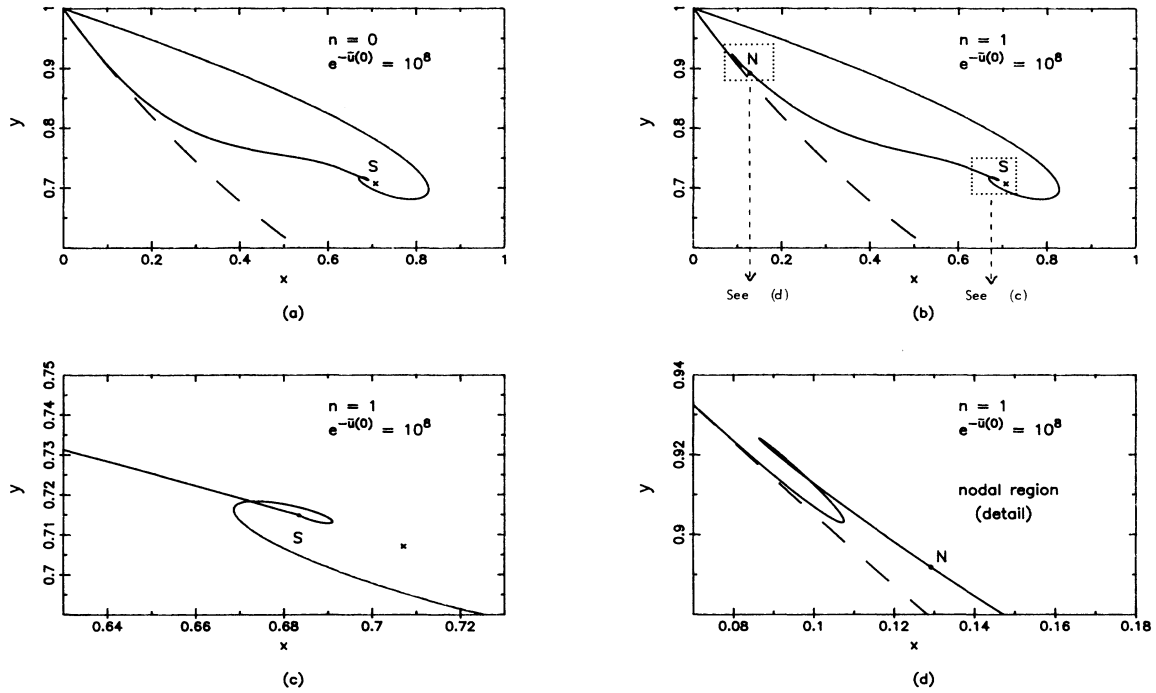

FIG. 11. The (x,y) trajectory for $n=0$ (a) and for $n=1$ (b)–(d) when the initial value $e^{-\bar{u}(0)}$ is large, $=10^8$. The point S denotes the scaling region and the cross indicates the critical point $x=y=2^{-1/2}$. The dashed curve is the Schwarzschild hyperbola and the point N in (b) and (d) denotes the node of the $n=1$ solution.

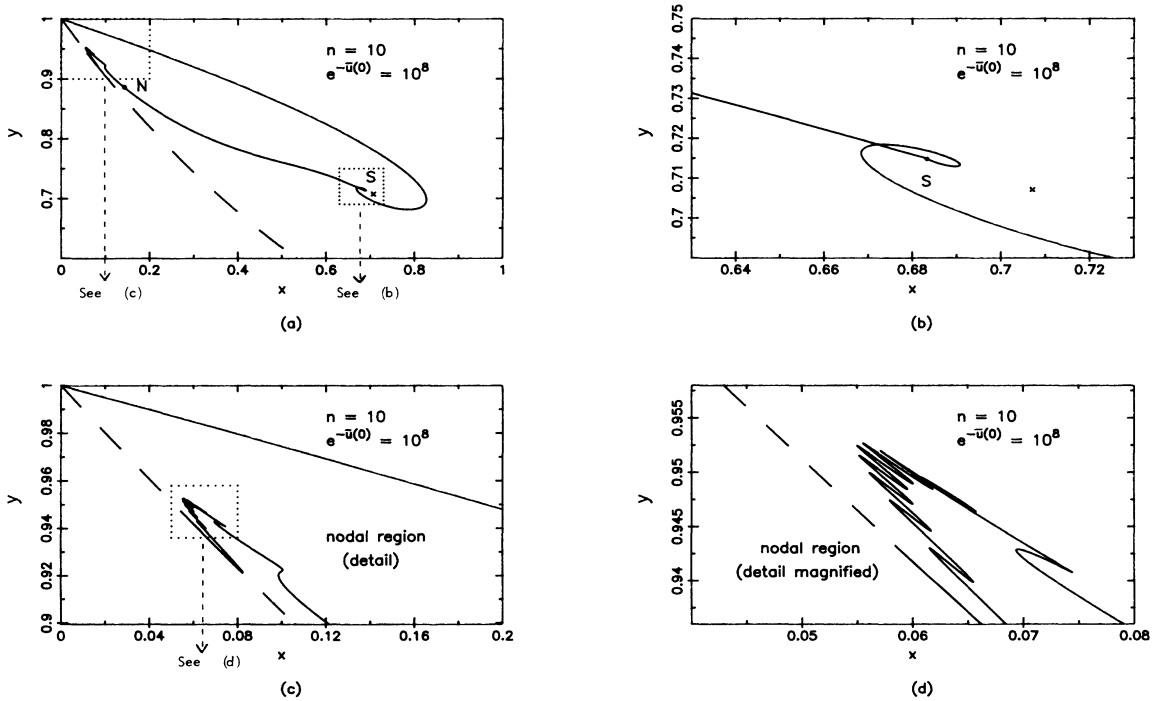

FIG. 12. The (x,y) trajectory for $n=10$ when the initial value $e^{-\bar{u}(0)}$ is large, $=10^8$. The points S and N denote the scaling region and the first node. The critical point $x=y=2^{-1/2}$ is indicated by a cross, and the dashed curve is the Schwarzschild hyperbola. Note the ten loops in (d); to see all the loops clearly, more magnification is required.

examples of (x,y) trajectories for $n=0$, 1, and 10 when

$$e^{-\bar{u}(0)}=10^8 . \tag{4.34}$$

We see that each trajectory now has $n+1$ extra loops (instead of the previous n). These solutions can be best understood by separating the trajectory into four fairly distinct regions.

(i) Central region. This extends from the origin

$$\rho=0 \text{ to } \rho\sim e^{\bar{u}(0)}/m \ll m^{-1} . \tag{4.35}$$

In this region, because $e^{-\bar{u}(0)}\gg 1$, the (x,y) trajectory stays very close to the W-dominating solution of (2.40), given by Fig. 3. In the case of $e^{-\bar{u}(0)}=10^8$, the central region refers to the portion beginning at the starting point $x=0, y=1$, covering the entire upper part of the trajectory and then extending counterclockwise to the lower part, up to the point S [in the middle of the *first* loop of Figs. 11(a), 11(b), and 12(a)].

Within this region, V rises from 0 to a value much larger than U, though it remains much smaller than W. It is useful to think of (2.6),

$$\frac{d}{d\rho}(W-U+V)=-\frac{4}{\rho}V-2(W+V)\frac{du}{d\rho} , \tag{4.36}$$

or equivalently

$$\frac{d}{d\rho}[(W-U+V)e^{2u}]=-e^{2u}\left[\frac{4}{\rho}V+2U\frac{du}{d\rho}\right] , \tag{4.37}$$

in terms of a mechanical analog. Imagine a point particle of "position" σ and "time" ρ, with a "kinetic energy" V and a "potential energy,"

$$W-U=\tfrac{1}{2}(e^{-2\bar{u}}-1)\sigma^2 . \tag{4.38}$$

The right-hand side of (4.36) may be regarded as a friction force. Because $du/d\rho$ and V are both >0, this force is always negative, like friction. Within a "time"

$$\rho\lesssim e^{\bar{u}(0)}/m ,$$

σ would slide down in the potential (4.38), converting part of the potential energy to kinetic; hence, V could rise to become much larger than U. This behavior is illustrated by the beginning parts of Figs. 13(a), 13(c), 13(d), and 14(a)–14(d). Because the W-dominating trajectory stops at its critical point (2.43), $(x,y)=(2^{-1/2},2^{-1/2})$, the central region ends at a point S quite close to that critical point [marked by a $\times$ in Figs. 11(a)–11(c) and 12(a) and 12(b)]. Let x_S and y_S be the coordinates of S. We may write

$$x_S=2^{-1/2}-\xi \text{ and } y_S=2^{-1/2}+\eta . \tag{4.39}$$

Both ξ and η are small; their relation will be analyzed below.

(ii) Scaling region. In the (x,y) plane, the scaling region refers essentially to the single point S (and its immediate neighborhood). At that point, the variables σ, u, W, V, U, and ρ all change substantially. Instead of the purely W-dominating central region, V now also plays a role.

Set, as an approximation,

$$\dot{x}=\dot{y}=0 \tag{4.40}$$

and

$$U=0 \tag{4.41}$$

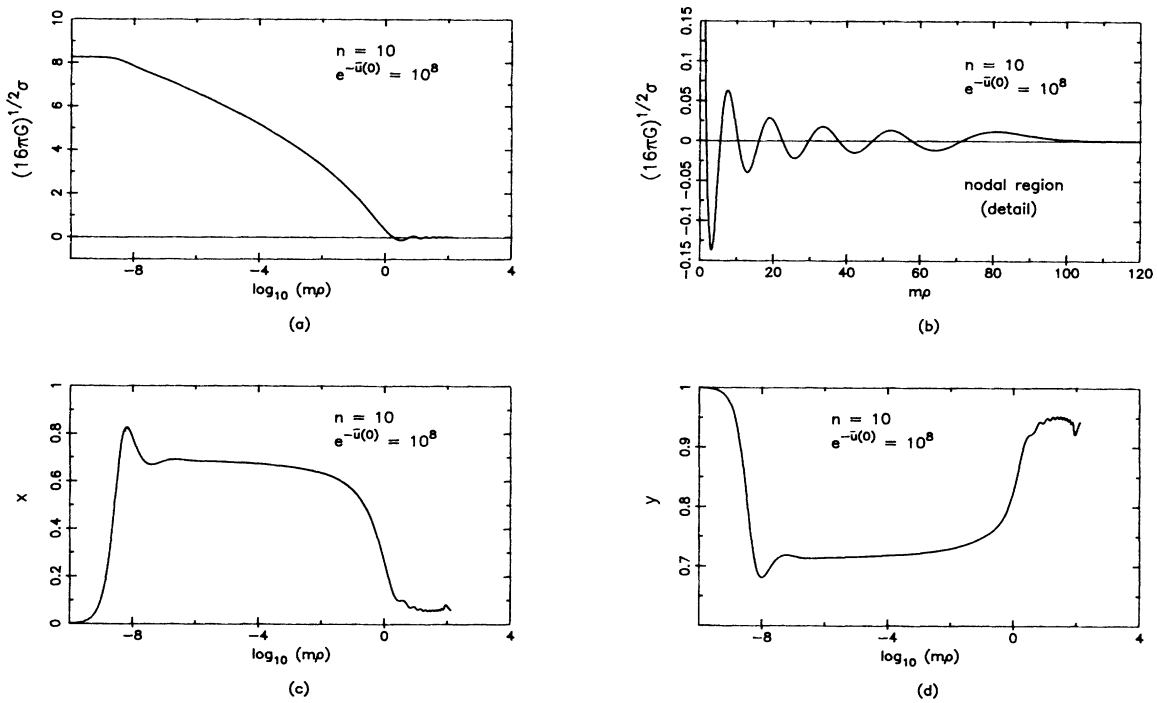

FIG. 13. Dependence of σ, x, and y on the radius ρ for the solution with ten nodes ($n=10$) and a large initial value $e^{-\bar{u}(0)}=10^8$.

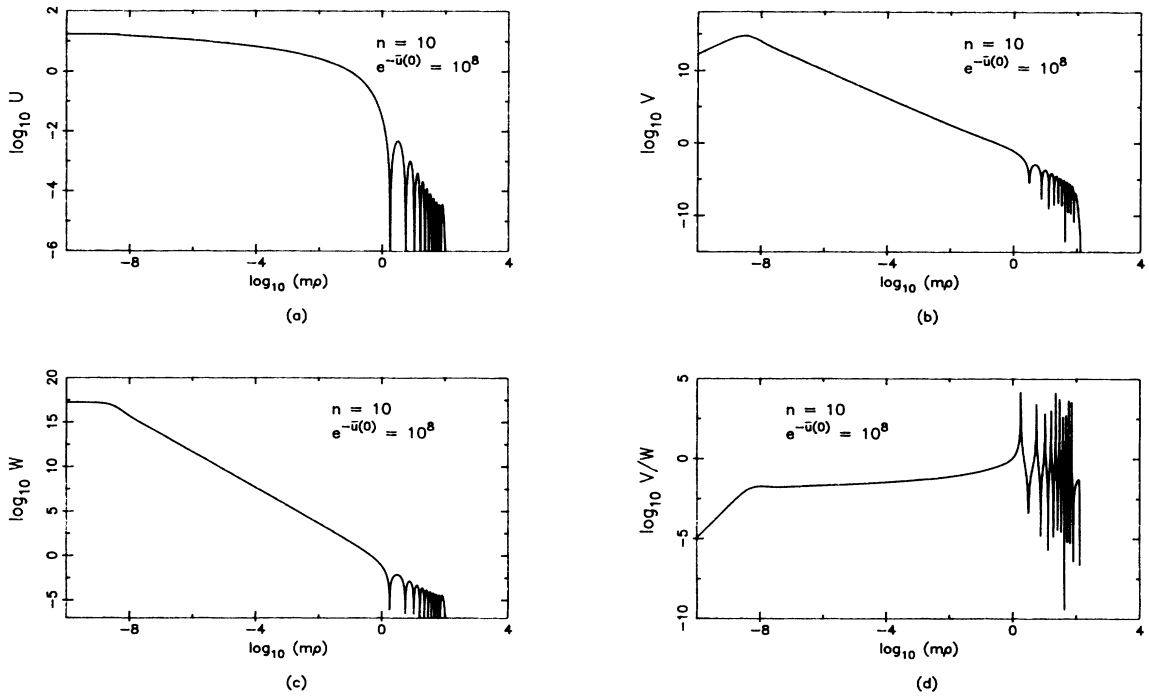

FIG. 14. The matter densities U, V, W, and the ratio V/W vs the radius ρ for the solution with $n=10$ and $e^{-\bar{u}(0)}=10^8$.

in (2.11)—(2.13). Equation (4.40) follows from the assumption that ρ changes, but the (x,y) trajectory remains at the point S; the second approximation (4.41) is made on account of U being much smaller than V and W. Hence,

$$1-y^2-xy=0\ , \tag{4.42}$$

$$V=(16\pi G)^{-1}(2xy-x^2+y^2-1)\rho^{-2}\ , \tag{4.43}$$

and

$$W=(16\pi G)^{-1}(x^2+1-y^2)\rho^{-2}\ . \tag{4.44}$$

From (4.40) and (2.9), one has

$$y=e^{-\bar{v}},\quad \frac{x}{y}=\rho\frac{du}{d\rho}$$

and therefore

$$e^u\propto\rho^{x/y}\ . \tag{4.45}$$

Because of (4.44),

$$W=\tfrac{1}{2}e^{-2u}\sigma^2\propto\rho^{-2}\ ; \tag{4.46}$$

it follows then that

$$\sigma\propto\rho^{(x-y)/y}\ . \tag{4.47}$$

Substituting (4.39) into (4.42) and (4.47), and neglecting quadratic terms in ξ and η, we have

$$\xi=2\eta \tag{4.48}$$

and

$$\sigma\propto 1-2^{1/2}(\xi+\eta)\ln(\rho m)\ . \tag{4.49}$$

Hence,

$$V=\tfrac{1}{2}e^{-2\bar{v}}\left[\frac{d\sigma}{d\rho}\right]^2\propto(\xi+\eta)^2\frac{1}{\rho^2}$$

and therefore V/W is a small constant, confirming (4.43). An examination of the middle parts of Figs. 13(a), 13(c), and 14(a)—14(d) shows that these formulas hold remarkably well, with $\eta\sim 0.1$ and $\xi\sim 0.2$ for the case $n=10$ and $e^{-\bar{u}(0)}=10^8$. The scaling region extends from $m\rho\sim\exp\bar{u}(0)\ll 1$ to $m\rho\sim 1$, when σ is near its first node.

(iii) Belly. When σ hits its first node, point N on the (x,y) trajectory in Figs. 11(b) and 12(a), the situation changes into the V-dominating region. At the node $\sigma=0$, and therefore

$$U=W=0$$

and (2.11)—(2.13) give

$$\begin{aligned}\dot{x}&=-x(x+y)\ ,\\ \dot{y}&=1-y^2-xy\ ,\\ \frac{dx}{dy}&=\frac{x^2+xy}{y^2+xy-1}\ .\end{aligned} \tag{4.50}$$

The (x,y) trajectory is forced from the scaling point S to take a swing in order to reach N, along (4.50). This forms the belly between S and N in Figs. 11(b) and 12(a). [The point N is absent in Fig. 11(a) since it refers to $n=0$, the no-node solution.]

(iv) Nodal region. Beyond the first node, $(16\pi G)^{1/2}\sigma$ is

TABLE II. Radius R, particle number N, and mass M at the first cusp $(n,1)$ when the number of nodes $n=0,1,\ldots,10$.

n	mR	Gm^2N	GmM
0	3.109 78	0.653 003	0.633 001
1	7.891 62	1.392 134	1.356 265
2	12.831 69	2.137 840	2.085 372
3	17.840 01	2.883 631	2.814 529
4	22.892 76	3.628 891	3.543 186
5	27.977 50	4.373 581	4.271 317
6	33.089 11	5.117 754	4.998 970
7	38.222 51	5.861 469	5.726 202
8	43.374 70	6.604 782	6.453 063
9	48.544 21	7.347 736	7.179 595
10	53.728 30	8.090 369	7.905 833

very small, and the solution resembles a corresponding Newtonian one, as can be seen from Figs. 13(a) and 13(b). This is perhaps the least interesting region.

E. Radius

The radius of a mini-soliton star may be defined by

$$R\equiv\frac{1}{M}4\pi\int_0^\infty (U+V+W)\rho^3 d\rho\ , \tag{4.51}$$

where, in accordance with the mass formula (2.23), M is given by

$$M=4\pi\int_0^\infty (U+V+W)\rho^2 d\rho\ .$$

The numerical values of the radius R, the particle number N, and the mass M at the first cusp $(n,1)$ are given in Table II for $n=0,1,\ldots,10$. As expected, they all increase with n. The ratio R/GM is plotted against N in Fig. 15(a), and against M in Fig. 15(b); both refer to values at the cusp $(n,1)$, and for $n=0,1,\ldots,56$. (Note that for the Schwarzschild radius the corresponding ratio is $R/GM=2$.)

We have also tried a different definition of the star radius, replacing (4.51) by

$$\frac{1}{M}8\pi\int_0^\infty (2W-U)e^{u+\bar{v}}\rho^3 d\rho\ , \tag{4.52}$$

where, in accordance with (2.27),

$$M=8\pi\int_0^\infty (2W-U)e^{u+\bar{v}}\rho^2 d\rho\ .$$

We find that the fractional difference between these two definitions of radius, (4.51) and (4.52), is only $\sim 10^{-2}$.

V. STABILITY

At each N, the ground-state stellar mass $M_{\min}(N)$ is given by the minimum of all $[M_n(N)]_{\min}$, which is also the $[M_n(N)]_{\min}$ with the smallest allowed n. Each of these ground state solutions is stable, except against fission, because inequalities such as

$$M_{\min}(N+N')>M_{\min}(N)+M_{\min}(N') \tag{5.1}$$

can occur. A complete survey of all possible N and N' lies outside the scope of this paper. Here, we will study only the $M_{\min}(N)$ vs N curve at the $(n,1)$ cusps for different $n=0,1,2,\ldots$. At each $(n,1)$ cusp we have

$$M_{\min}=M(n,1)$$

and (5.2)

$$N=N(n,1)\ .$$

For $n=0,1,\ldots,10$, (4.17) can be written as

$$M_{\min}(N)=m(1-0.022\,173)N -(Gm)^{-1}[5.232\times10^{-3}+\delta(N)]\ , \tag{5.3}$$

which gives

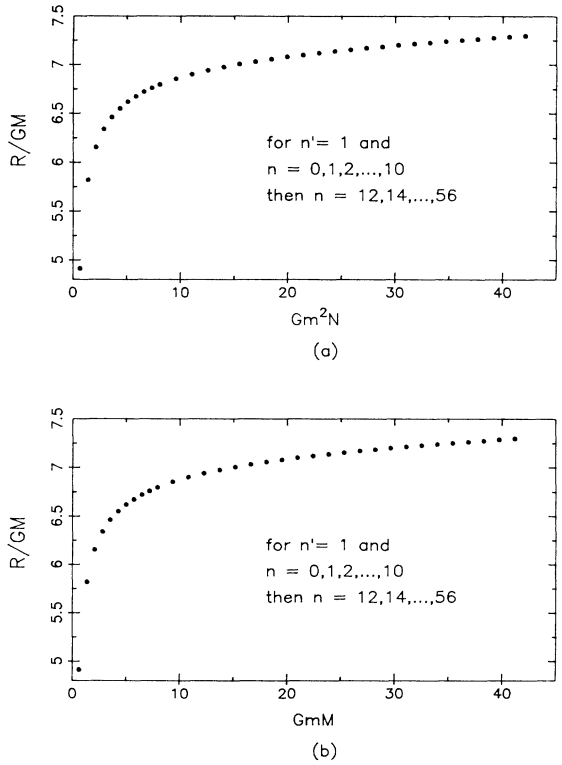

FIG. 15. Plot of R/GM vs N (a) and vs M (b) at the cusp $(n,1)$ for $n=0,1,2,\ldots,56$.

$$[M_{\min}(N+N')-M_{\min}(N)-M_{\min}(N')]Gm=5.232\times10^{-3}-\delta(N+N')+\delta(N)+\delta(N')>0\ , \tag{5.4}$$

since δ is $\sim10^{-4}$. Consequently, for $n=0,1,\ldots,10$ the inequality (5.1) holds, and a large n mini-soliton star is unstable against fission.

For larger n, up to 56, we may use (4.18) and denote the correction term there as $\epsilon(N)$. This gives

$$[M_{\min}(N+N')-M_{\min}(N)-M_{\min}(N')]Gm=1.8542\times10^{-2}-1.3750\times10^{-2}(e^{-\alpha Gm^2N}+e^{-\alpha Gm^2N'}-e^{-\alpha Gm^2(N+N')})$$
$$-\epsilon(N+N')+\epsilon(N)+\epsilon(N')\ , \tag{5.5}$$

where $\alpha=5.81\times10^{-2}$ and $\epsilon(N)$ is $\sim10^{-5}$, given in Fig. 6. The sum inside the first set of parentheses on the right-hand side is

$$1-(1-e^{-\alpha Gm^2N})(1-e^{-\alpha Gm^2N'})\ ,$$

which lies between 0 and 1. Thus, (5.1) holds, indicating instability against fission. The no-node solution $[M_0(N)]_{\min}$ is, of course, absolutely stable.

Apart from fission by increasing the number of nodes n indefinitely, there does not seem to be an upper bound in mass for the mini-soliton stars.

ACKNOWLEDGMENTS

One of us (T.D.L.) wishes to thank the members of the CERN Theory Division for their kind hospitality when most of this paper was written. This research was supported in part by the U.S. Department of Energy.

APPENDIX

To establish the time dependence of ϕ for the lowest-energy solution at a fixed particle number N, we write

$$\phi=(\phi_R+i\phi_I)/\sqrt{2}\ , \tag{A1}$$

where ϕ_R and ϕ_I are both real. Setting the superscript $\mu=0$ in (1.26), we have

$$j^0=-ie^{-2u}\left[\phi^\dagger\frac{\partial\phi}{\partial t}-\frac{\partial\phi^\dagger}{\partial t}\phi\right]\ . \tag{A2}$$

Denote

$$\dot\phi_R=\frac{\partial\phi_R}{\partial t}\quad\text{and}\quad\dot\phi_I=\frac{\partial\phi_I}{\partial t}\ . \tag{A3}$$

In accordance with (1.37), N becomes

$$N=\int e^{-2u}(\phi_R\dot\phi_I-\phi_I\dot\phi_R)\,|g|^{1/2}dx^1dx^2dx^3\ . \tag{A4}$$

The energy of the system is

$$E=E(m)+E(g)\ , \tag{A5}$$

where $E(g)$ is given by (1.22) and is independent of ϕ. As in (1.38), the matter-energy $E(m)$ can be written as

$$E(m)=\int(U+V+W)\,|g|^{1/2}dx^1dx^2dx^3\ , \tag{A6}$$

where U and V are independent of $\dot\phi_R$ and $\dot\phi_I$ and W is

$$W=\tfrac{1}{2}e^{-2u}(\dot\phi_R{}^2+\dot\phi_I{}^2)\ . \tag{A7}$$

At any time t, assuming that ϕ_R, ϕ_I, and N are given, we wish to find the $\dot\phi_R$ and $\dot\phi_I$ which make E minimum. Consider an infinitesimal variation

$$\dot\phi_R\to\dot\phi_R+\delta\dot\phi_R$$

and (A8)

$$\dot\phi_I\to\dot\phi_I+\delta\dot\phi_I\ ,$$

keeping ϕ_R, ϕ_I, and the metric $g_{\mu\nu}$ fixed. The minimum energy solution is determined by

$$\delta(E+\omega N)=0\ , \tag{A9}$$

where ω is the Lagrange multiplier. This leads to

$$\dot\phi_R=\omega\phi_I,\quad\dot\phi_I=-\omega\phi_R\ , \tag{A10}$$

and therefore

$$\phi\propto e^{-i\omega t}\ , \tag{A11}$$

which is (1.30).

Note that the validity of this conclusion is independent of the complexity of the nonlinear interaction $U(\phi)$, and of the interaction between $g_{\mu\nu}$ and ϕ.

[1]T. D. Lee, preceding paper, Phys. Rev. D 35, 3637 (1987), hereafter referred to as I.

[2]G. W. Gibbons and S. W. Hawking, Phys. Rev. D 15, 2753 (1977).

[3]See Ref. 16 of I.

[4]R. Arnowitt, S. Deser, and C. W. Misner, in *Gravitation: An Introduction to Current Research*, edited by L. Witten (Wiley-Interscience, New York, 1962), p. 227.

[5]R. Friedberg, T. D. Lee, and Y. Pang, following paper, Phys. Rev. D 35, 3658 (1987).